High-Density Plasma Production in Converging Field Following a Magnetic Beach Plasma Source*)

Atsushi OKAMOTO, Ryosuke OCHIAI, Katsuya SATOU, Hiroki HACHIKUBO, Minami SUGIMOTO, Takaaki FUJITA and Hiroyuki TAKAHASHI[1)]

Nagoya University, Nagoya 464-8603, Japan
[1)]*Tohoku University, Sendai 980-8579, Japan*

(Received 28 September 2018 / Accepted 16 November 2018)

A high ion saturation current (I_{is}) phase, which is characterized by larger increase/decrease of I_{is} compared with the magnetic field variation, is observed in a converging field following an electron cyclotron resonance plasma source with a magnetic beach configuration. Plasma production rate and particle influx are considered in terms of orbits of collisionless electrons. While the ionization probability of one-pass electron is order of 0.1, the mirror trapped electron cause ionization within several or dozen bouncing. This is an essence of improved ionization rate resulting in the high I_{is} phase. The temporal evolution of ion saturation current observed in the experiment is well explained by the estimated plasma production rate and particle influx.

Keywords: electron cyclotron resonance, magnetic beach configuration, converging magnetic field, bounce motion, pitch angle, high-density plasma

DOI: 10.1585/pfr.14.2401005

1. Introduction

Plasmas in open field lines are widely utilized to fusion studies on divertor plasma physics [1–4], and wave interaction with energetic ion [5]. An advantage using linear devices for such studies is independent controllability of plasma production. In terms of electron energy controllability, the electron cyclotron resonance (ECR) with magnetic beach configuration is a suitable method for a plasma source [6]. Also the ECR with a microwave injected along the field line in magnetic beach configuration enables us to produce an overdense plasma [7]. Therefore the ECR plasma production is a candidate for those studies using linear devices. On the other hand, the ECR condition restricts the magnetic field in the production region, while various and sometimes higher magnetic fields are required for target or test regions. Then the device consists of a production region with weaker magnetic field and a test region with higher magnetic field; plasmas in the production region are supplied to the test region through a converging magnetic field.

We have developed such a linear device with an ECR plasma source [8]. While the first plasma was successfully produced, a transition phenomenon was observed in the ion saturation current. In order to establish a high-density operation required for divertor plasma and energetic ion studies, utilizing the transition phenomenon is significant. In this paper, investigation of the phenomenon in terms of ionization and plasma supplying through a converging field region is described.

2. Experimental Setup

The experiments were performed using a linear plasma device, Nagoya University Magnetoplasma Basic Experiment (NUMBER), which consists of an ECR plasma production region and a test region supplying target plasmas for studies on divertor plasma and energetic ion as shown in Fig. 1. A vacuum chamber made of stainless steel has dimensions of 0.2 m in diameter and 1.8 m in axial length. Helium gas is used in the present experiments,

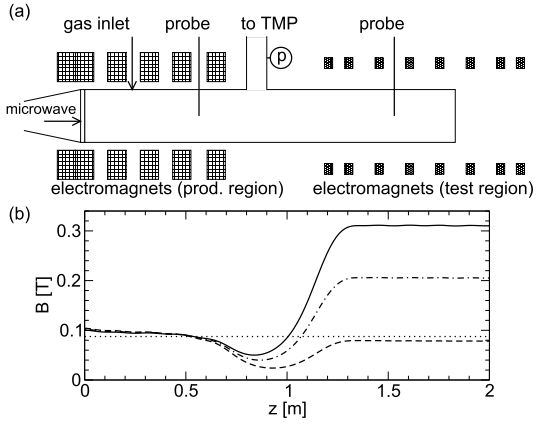

Fig. 1 (a) Schematic of experimental setup and (b) magnetic field on the axis, where solid curve represents that at t = 12 ms, dashed-dotted curve at t = 30 ms, broken curve at t = 70 ms. Dotted line corresponds to $B = B_{ECR}$.

author's e-mail: okamoto.atsushi@nagoya-u.jp

*) This article is based on the presentation at the 12th International Conference on Open Magnetic Systems for Plasma Confinement (OS2018).

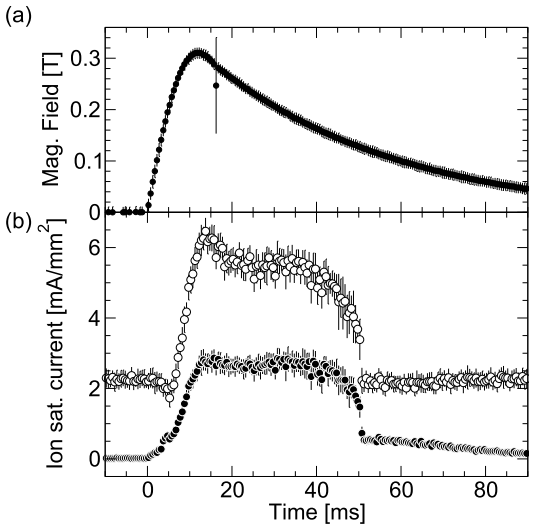

Fig. 2 Typical temporal evolution of (a) magnetic field in the test region and (b) ion saturation currents. Open circles represent that measured at the production region, while filled circles at the test region.

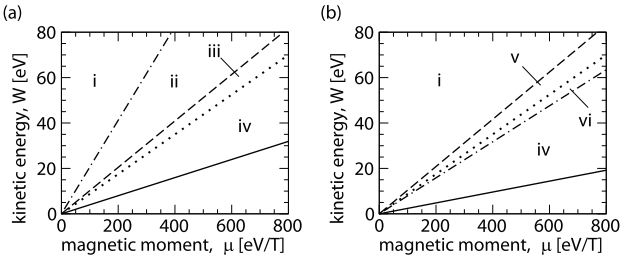

Fig. 3 Classification of electron orbits in μ-W space at (a) t = 30 ms and (b) t = 70 ms. Solid lines correspond to the location of minimum magnetic field, $B_{\rm min}$; dotted lines, that of resonance, $B_{\rm ECR}$; broken lines, that of the microwave injection window, B_0; dashed-dotted lines, that of the test region, $B_{\rm test}$.

which is continuously fed into the production region and is pumped out from a pumping duct between the production region and the test region. Working pressure is about 0.2 Pa.

The plasma is produced by the electron cyclotron resonance (ECR) with a microwave, which is injected along the magnetic field through a quartz window from an end of the device. Frequency and injected power of the microwave are $f = \omega/2\pi = 2.45$ GHz and $P = 2.8$ kW. The magnetic field at the window $B_0 \simeq 0.1$ T satisfies a high field side condition, $B_0 > B_{\rm ECR} \equiv \omega m_{\rm e}/e$, where $m_{\rm e}$ and e represent the electron mass and the elementary charge. Magnetic field in the production region consists of a magnetic beach; it matches $B = B_{\rm ECR}$ in the middle of the production region.

The magnetic field in the test region is uniform and is up to $B_{\rm test} = 0.3$ T. The magnetic coil current for the test region is supplied by a capacitor bank, flat top duration of which is about 4 ms as shown in Fig. 2 (a).

Those two regions are longitudinally connected to each other. Since the magnetic beach configuration matches with the ECR condition, a local minimum of magnetic field exists between these two regions making a magnetic mirror before entering the test region.

Langmuir probe measurements are applied both in the production region ($z = 0.57$ m) and the test region ($z = 1.53$ m), where z is a distance from the microwave injection window. Typical electron temperature and density are $T_{\rm e} = 4$ eV and $n_{\rm e} = 5 \times 10^{17}$ m^{-3} in the test region, while $T_{\rm e} = 5$ eV and $n_{\rm e} = 8 \times 10^{17}$ m^{-3} in the production region [8].

3. Results and Discussion

Temporal evolution of ion saturation currents ($I_{\rm is}$) are plotted with that of the magnetic field in the test region in Fig. 2. Before the discharge circuit of capacitor bank turns on, $t < 0$, magnetic field is only applied in the production region; a steady state plasma is produced in the production region with continuous microwave injection. Then, ion saturation current is only observed in the production region as shown in Fig. 2 (b).

The magnetic field rises up to $B_{\rm test} \simeq 0.3$ T after the discharge circuit turns on at $t = 0$. Then it gradually decreases owing to a crowbar circuit as shown in Fig. 2 (a). We note that a deviation at $t = 16$ ms is caused by a stray inductance of the crowbar circuit. The ion saturation current in the test region gradually increases as the magnetic field increases. At about $t \simeq 6$ ms, large increase of ion saturation current is observed both in the production and the test regions. Then the both currents are kept almost constant while the magnetic field in the test region gradually decreases; $t \simeq 12$ - 50 ms. This phase is hereafter referred to as "high $I_{\rm is}$ phase".

Large decrease of the ion saturation currents are observed both in the production and the test regions at about $t \simeq 50$ ms. After the large decrease of the currents, the current is kept constant in the production region as well as that before the discharge circuit turns on. Ion saturation current in the test region gradually decreases with the magnetic field in the test region. This phase is hereafter referred to as "low $I_{\rm is}$ phase".

While the temporal evolution of ion saturation current in the test region responds to variation of the local magnetic field in the low $I_{\rm is}$ phase, it is almost independent of the magnetic field in the high $I_{\rm is}$ phase. To understand these phenomena in terms of plasma production in these magnetic configurations, classification of electron orbit in μ-W diagram is discussed in the followings.

Since the kinetic energy $W = m_{\rm e}{v_\parallel}^2/2 + m_{\rm e}{v_\perp}^2/2$ and the magnetic moment $\mu = (m_{\rm e}{v_\perp}^2/2)/B$ are constants for collisionless electrons, those electrons correspond to fixed points in the μ-W diagram shown in Fig. 3. In the expressions above, $v_\parallel$ and $v_\perp$ denote parallel and perpendicular

velocities of an electron. An effect of electrostatic potential variation along the magnetic field line is omitted for simplicity. The parallel energy $W_{\parallel}(z) = m_e {v_{\parallel}}^2/2$ of an electron with (μ, W) at a specific position z is indicated as a vertical displacement from the line $W = B(z)\,\mu$ to the point (μ, W). Therefore, there are no electrons below the line $W = B_{\min}\,\mu$, which corresponds to the lowest magnetic field.

Orbits of electron moving along the magnetic field are classified by the region (i)-(vi) indicated in Fig. 3. In region (i), electrons freely move from the production region to the test region and vice versa, resulting in loss at both ends of the device. Part of these electrons plays particle influx for the test region.

In region (ii), electrons are prohibited to enter into the test region due to a magnetic mirror in front of the test region. These electrons disappear when they reach to the microwave injection window.

Region (iii) contains the electrons that match to the ECR condition, gaining energy from microwave. Also the electrons suffer from the magnetic mirror reflections in front of both the microwave injection window and the test region. Therefore, the electrons bounce between the mirrors resulting in ionization and plasma production.

In region (iv), electrons are mirror trapped as well as those in region (iii). However, no electrons satisfy the resonant condition in this region.

Region (v) appears when the magnetic field strength in the test region is smaller than that at the microwave injection window as shown in Fig. 3 (b). In this case, electrons escape only to the test region playing the particle influx. In addition, a part of the electrons in this region can gain the energy from microwave. Ionization efficiency, however, is relatively lower than that in region (iii) because electrons in region (v) are not confined unlike the mirror-confined electrons in region (iii).

Electrons in region (vi) also escape only to the test region as those in region (v), but no resonant condition.

When an isotropic distribution of electrons is considered, the electrons equally occupy the velocity ($\boldsymbol{v}$-) space. Since the magnetic moment $\mu = m_e {v_{\perp}}^2/2B = (m_e v^2/2B)[1 - (v_{\parallel}/v)^2] = (m_e v^2/2B)\sin^2\chi$ at a specific position is a function of the pitch angle $\chi \equiv \arccos(v_{\parallel}/v)$, we can consider a distribution in μ space. The cumulative distribution function in μ space is considered:

$$G(\mu) \equiv \int_0^{\mu} g_{\mu}(\mu')\mathrm{d}\mu' = \int_0^{\chi(\mu)} g_{\mu}(\mu')\frac{\mathrm{d}\mu'}{\mathrm{d}\chi}\mathrm{d}\chi, \qquad (1)$$

where $g_{\mu}(\mu)$ is a probability density function in μ space. Apparently, for a given kinetic energy W_0 of electrons at the position of minimum magnetic field $B_{\min}$, $G(0) = 0$ and $G(W_0/B_{\min}) = 1$. Recalling that $\mathrm{d}\mu/\mathrm{d}\chi = (m_e v^2/B)\sin\chi\cos\chi$ and $\int_0^{\pi/2}\sin\chi\mathrm{d}\chi = 1$, we find that $g_{\mu}(\mu) = (B/m_e v)(1/\cos\chi)$. Then $G(\mu) = 1 - \sqrt{1 - \mu B_{\min}/W_0}$ is obtained. A fraction of electrons belonging to a region that corresponds to $B_1 < B < B_2$ is given by $G(W_0/B_1) - G(W_0/B_2)$. Figure 4 shows a temporal variation of those fractions at the minimum magnetic field position under the assumption of the isotropic distribution in $\boldsymbol{v}$-space. More than 65% of the electrons are in region (iv): mirror trapped without resonant condition, which does not contribute to particle supplying to the test region nor to ionization. Plasma production or electron-collision ionization are dominated by the electrons in regions (iii) and (v). Fractions of those electrons are almost constant but slightly larger for higher magnetic field.

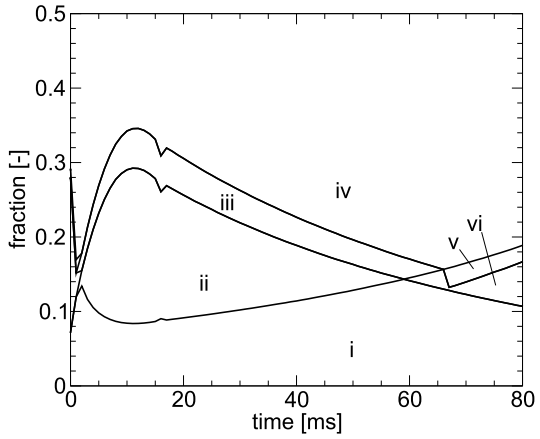

Fig. 4 Cumulative fraction of electron orbit based on the magnetic field variation in the experiment.

The resonant electrons with bounce motion, which are classified as region (iii), have an advantage in plasma production compared to the resonant electrons in the loss cone, region (v). We can assume that the energy obtained by an electron for an interaction with the microwave is higher than that of the ionization potential. Ionization frequencies for the present experiment are $\nu_i \simeq 1.8 \times 10^5\ \mathrm{s}^{-1}$ for an electron with kinetic energy $W = 40\,\mathrm{eV}$, for example, and $\nu_i \simeq 0.9 \times 10^5\ \mathrm{s}^{-1}$ for $W = 100 - 1000\,\mathrm{eV}$ electrons. Bouncing period for those electrons are $T_b = 0.4\,\mu\mathrm{s}$ ($W = 40\,\mathrm{eV}$), $0.25\,\mu\mathrm{s}$ (100 eV), and $0.08\,\mu\mathrm{s}$ (1 keV). Probabilities of the ionization for one bounce motion are $\nu_i T_b = 0.07, 0.2,$ and 0.07, respectively. For untrapped resonant electrons in region (v), electron transit time $\tau \sim L/v$ is similar to T_b of the trapped electron. Probability of the ionization by the untrapped resonant electrons in region (v) is also $\nu_i\tau \sim 0.1$; only about 10% of electrons contribute to ionize. Majority of the untrapped resonant electrons escape to the end of device without consuming their energy gaining from microwave. It is therefore difficult to ionize in a single pass. For the trapped and resonant electrons in region (iii), on the other hand, about several or dozen times bouncing enables the electrons to contribute to ionize resulting in efficient energy transfer from the microwave to the plasma production. We can consider ionization efficiency in region (iii) is about one order higher than that in region (v).

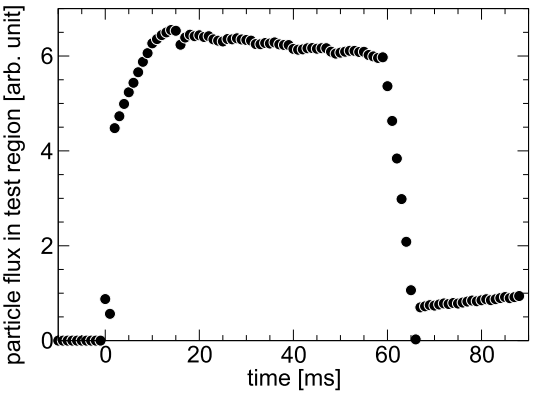

Fig. 5 Particle flux flowing to the test region.

In terms of supplying particles to the test region, fractions of a part of the region (i) and whole of the regions (v) and (vi) are important. The particle supply reaches the minimum when the magnetic field is the maximum ($t \simeq 12$ ms) due to the highest mirror ratio at the entrance of the test region. It gradually increase as long as the magnetic field in the test region is higher than that at the microwave injection window.

Taking above discussion account, particle flux flowing into the test region is plotted in Fig. 5. The particle flux is proportional to the product of two fractions: the fraction of regions (iii) and (v) ionizing and producing plasma, and the fraction of a part of the region (i) and whole of the regions (v) and (vi) supplying particles to the test region. For electrons in region (iii) and (v), 100% and 10% ionization probabilities are assumed; ionization rate is proportional to $S = f_{(\mathrm{iii})} + 0.1 f_{(\mathrm{v})}$, where f_n is the fraction in region n. Half of electrons in region (i) are assumed to be supplied into the test region, while the rest lose at the microwave injection window; $T = 0.5 f_{(\mathrm{i})} + f_{(\mathrm{v})} + f_{(\mathrm{vi})}$ represents a transport factor to the test region. Then we can see transitional increase and decrease of the particle flux Γ, which is proportional to $\Gamma = ST$, as shown in Fig. 5. Almost constant flux is supplied to the test region while the magnetic field gradually decreases for $t \simeq 10$ - 60 ms. This is because almost constant ionization fraction in this phase and particle supplying fraction as indicated in Fig. 4.

The behavior well corresponds to the ion saturation current in the test region shown by filled circles in Fig. 2 (b) except for some differences in detail. Time scales of the large increase/decrease are similar between the particle flux in Fig. 5 and I_{is} in Fig. 2 (b). Absolute value of the transition time to the high I_{is} phase is slightly earlier and that to the low I_{is} phase is slightly latter for the particle flux in Fig. 5. In the present study, we assume that the resonant condition of ECR is satisfied for all electrons in regions (iii) and (v). For more detailed discussion, the resonant condition should be restricted: only the electrons on the line $W = B_{\mathrm{ECR}}\,\mu$ in Fig. 3 match the resonant condition $\omega = \omega_{\mathrm{ce}}$ for stationary case. Otherwise we have to consider the Doppler-shifted resonant condition, $\omega - \omega_{\mathrm{ce}} - k v_{\parallel} = 0$, instead, where k represents the wavenumber of electron cyclotron wave propagating along the magnetic field. Those conditions only occupy a part of regions (iii) and (v). This restriction of the resonant condition will cause the slight difference in transition timing.

As for behavior in the low I_{is} phase, showing constant in Fig. 5 is a particle flux passing through the entrance of the test region while the ion saturation current is measured in the middle of the test region. The ion saturation current is therefore determined by the flux along magnetic field and radial diffusion. This is a possible reason for the difference because weaker magnetic field causes larger radial diffusion in general.

As discussed above, detailed modeling will be required for quantitative understanding of formation of the high I_{is} phase and remains as our future works. However, trapping of the resonant electron between the magnetic mirrors and consequent increasing of ionization efficiency is an essence of the high I_{is} phase as indicated with a simple model of electron orbit classification.

4. Summary

A high ion saturation current (I_{is}) phase, which is characterized by larger increase/decrease of I_{is} compared with the magnetic field variation, is observed in a converging field following an electron cyclotron resonance plasma source with a magnetic beach configuration. Plasma production rate and particle influx are considered in terms of orbits of collisionless electrons. While the ionization probability of one-pass electron is order of 0.1, the mirror trapped electron cause ionization within several or dozen bouncing. This is an essence of improved ionization rate resulting in the high I_{is} phase. The temporal evolution of ion saturation current observed in the experiment is well explained by the estimated plasma production rate and particle influx.

Acknowledgments

The work was partly supported by MEXT/JSPS KAKENHI Grant Number JP17H06231.

[1] N. Ohno *et al.*, Nucl. Fusion **41**, 1055 (2001).
[2] E.M. Hollmann *et al.*, Phys. Plasmas **9**, 1226 (2002).
[3] A. Okamoto *et al.*, J. Nucl. Mater. **363-365**, 395 (2007).
[4] H. Takahashi *et al.*, Phys. Plasmas **23**, 112510 (2016).
[5] Y. Zhang *et al.*, Phys. Plasmas **15**, 102112 (2008).
[6] H. Shoyama *et al.*, J. Phys. Soc. Jpn. **65**, 2860 (1996).
[7] M. Tanaka *et al.*, J. Phys. Soc. Jpn. **60**, 1600 (1991).
[8] D. Hamada *et al.*, Plasma Fusion Res. **13**, 3401044 (2018).